# Energy-Efficient and High-Speed Dynamic Biped Locomotion Based on Principle of Parametric Excitation

Fumihiko Asano, *Member, IEEE*, and Zhi-Wei Luo, *Member, IEEE*

***Abstract*—We clarified that the common necessary condition for generating a dynamic gait results from the requirement to restore mechanical energy through studies on passive dynamic walking mechanisms. This paper proposes a novel method of generating a dynamic gait that can be found in the mechanism of a swing inspired by the principle of parametric excitation using telescopic leg actuation. We first introduce a simple underactuated biped model with telescopic legs and semicircular feet and propose a law to control the telescopic leg motion. We found that a high-speed dynamic bipedal gait can easily be generated by only pumping the swing leg mass. We then conducted parametric studies by adjusting the control and physical parameters and determined how well the basic gait performed by introducing some performance indexes. Improvements in energy efficiency by using an elastic-element effect were also numerically investigated. Further, we theoretically proved that semicircular feet have a mechanism that decreases the energy dissipated by heel-strike collisions. We provide insights throughout this paper into how zero-moment-point-free robots can generate a novel biped gait.**

***Index Terms*—Dynamic bipedal walking, efficiency, gait generation, mechanical energy, parametric excitation.**

## I. Introduction

HUMAN biped locomotion is an ultimate style of biological movement that is a highly evolved function. Biped locomotion by robots is a dream to be attained by the most highly evolved or integrated technology, and research on this has a history of over 30 years.

Many methods of generating gaits have been proposed, and several advanced approaches have taken the robot's dynamics into account. Miura and Shimoyama studied dynamic bipedal walking without ankle joint actuation [1], and developed robots on stilts whose foot contact occurred at a point. Sano and Furusho accomplished natural dynamic biped walking based on angular momentum using ankle joint actuation [2]. Kajita proposed a method of control based on a linear inverted pendulum model with a potential-energy-conserving orbit [3]. There has been a tendency to reduce the complicated dynamics of a walking robot to a simple inverted pendulum [4], and to control its motion according to predesigned time-dependent trajectories while guaranteeing zero moment point (ZMP) conditions [5]. In other words, biped robots must be precisely controlled actuating the ankle joints so that the ZMP remains in the sole during the walking. Although such approaches have successfully been applied to practical applications, serious problems still remain.

McGeer's passive dynamic walking (PDW) [6] has provided clues to solve these problems. Passive-dynamic walkers can walk without any actuation on a gentle slope, and they provide an optimal solution to the problem of generating a natural and energy-efficient gait. The objective most expected to be met by PDW is to attain natural, high-speed energy-efficient dynamic bipedal walking on level ground like humans do. By applying the properties of PDW, in the recent decade, walkers that are energy-efficient, high-speed, and human-like have been developed [7]. However, they need to supply power input to the robot by driving its joint actuators to continue stable walking on level ground, and certain methods of supplying power must be introduced.

Ankle joint torque is mathematically very important for effectively propelling the robot's center of mass (CoM) in the walking direction, and it is thus required relatively more often than other joint torques. However, to exert ankle joint torque on a passive-dynamic walker, we need to add feet and this creates the ZMP constraint problem. We clarified that there is a tradeoff between optimal gait and ZMP conditions through parametric studies, and concluded that generating an energy-efficient and high-speed dynamic biped gait is difficult using approaches based on ankle joint actuation [8], [9]. Utilizing the torso can be considered to solve this problem, and we should use the joint torques between the torso, stance, and swing leg. Another difficulty, however, then arises as to how to drive the legs while stably balancing the torso. This problem was investigated by Kinugasa [10].

A question then arises as to how to generate energy-efficient and high-speed dynamic biped locomotion without taking ZMP conditions into account or controlling the torso balance. This question further leads us to conclusion that if the leg itself has a mechanism to increase mechanical energy, these difficulties can be overcome. The answer can be found in the principle of parametric excitation. Minakata and Tadakuma experimentally demonstrated that level dynamic walking could be accomplished by pumping the leg [11]. This suggests that a dynamic

Manuscript received December 28, 2007; revised July 5, 2008. First published October 28, 2008; current version published December 30, 2008. This paper was recommended for publication by Associate Editor K. Hosoda and Editor H. Arai upon evaluation of the reviewers' comments. This work was supported in part by the Japan Society for the Promotion of Science (JSPS) under Grant-in-Aid for Scientific Research (B) 18360115.

F. Asano is with the Bio-Mimetic Control Research Group, Institute of Physical and Chemical Research (RIKEN), Nagoya 463-0003, Japan (e-mail: asano@bmc.riken.jp).

Z.-W. Luo is with the Bio-Mimetic Control Research Group, Institute of Physical and Chemical Research (RIKEN), Nagoya 463-0003, Japan, and also with the Department of Computer Science and Systems Engineering, Graduate School of Engineering, Kobe University, Kobe 657-8501, Japan (e-mail: luo@gold.kobe-u.ac.jp).

Digital Object Identifier 10.1109/TRO.2008.2006234

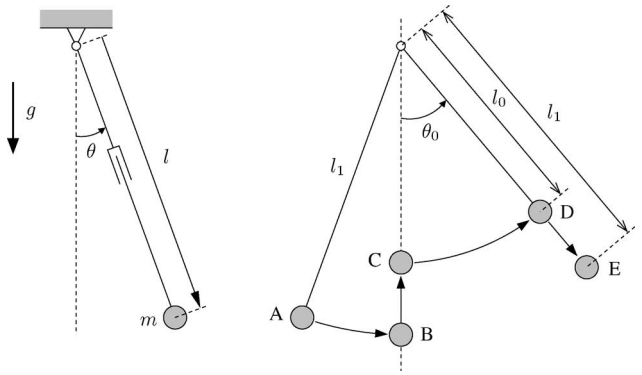


Fig. 1. (Left) Swing–person system and (right) optimal control to increase mechanical energy.

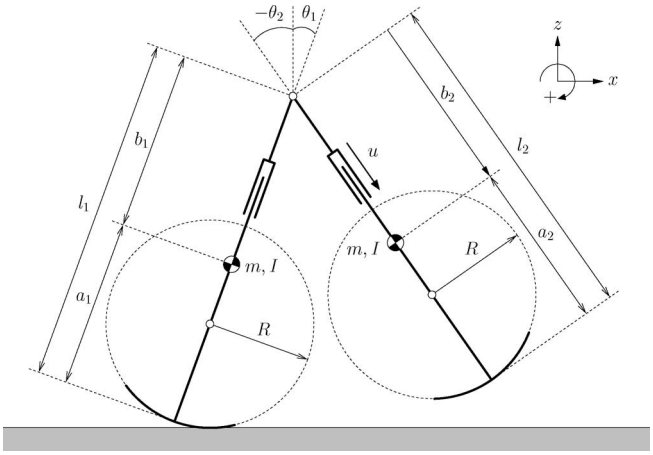


Fig. 2. Model of planar telescopic legged biped with semicircular feet.

biped gait can be generated without any rotational actuation, merely by pumping the motion of the leg. This mechanism can be understood as the effect of parametric excitation from the mechanical energy point of view, but the detailed mechanical principles underlying it have yet to be clarified.

Based on the observations, we propose a novel approach to biped gait generation based on the principle of parametric excitation. We introduce a simple control law for a planar telescopic legged biped model, and show that level gait generation can be easily accomplished by pumping the swing leg without taking ZMP conditions into account. We further numerically investigate what effects the system parameters had on the efficiency of dynamic gait. Our biped model has semicircular feet, which characterize passive-dynamic walkers, and they are very important for generating an efficient gait. It is thus theoretically investigated how mechanical energy dissipation caused by heel strikes is reduced in accordance with the foot radius. The authors provide novel insights on biped walking control in *ZMP-free robots* throughout this paper.

The remainder of this paper is organized as follows. In Section II, the principle of parametric excitation and its optimal control to increase mechanical energy are described. In Section III, a planar biped model with telescopic legs is introduced. In Section IV, it is numerically shown that level gait generation based on parametric excitation is possible by pumping the swing leg. In Section V, parameter study is conducted to clarify how the system parameters influence the efficiency. In the subsequent sections, the effects of elastic elements and semicircular feet on improvement of the energy efficiency are theoretically investigated. Finally, Section IX concludes the paper.

## II. Parametric Excitation Mechanism

Fig. 1 has a model of a swing–person system; point mass $m$ has a variable-length pendulum whose mass and inertia moment can be neglected. Here, $\theta$ (in radians) is the anticlockwise angle of deviation for the pendulum from the vertical and $g = 9.81$ m/s$^2$ is the gravity acceleration. Let

$$l_0 \leq l \leq l_1 \tag{1}$$

$$-\pi \leq \theta \leq \pi \tag{2}$$

where $l_0$ and $l_1$ (in meters) are constant, and $l_1 > l_0$. The proof for optimal control to increase mechanical energy can be described as follows. Let $L$ (in kilograms square meter per second) be the angular momentum of the system, which is given by

$$L = ml^2\dot{\theta} \tag{3}$$

and its time derivative satisfies the relation

$$\dot{L} = -mgl \sin\,\theta. \tag{4}$$

According to this, the optimal control to increase mechanical energy is

$$l = \begin{cases} l_1, & \text{for } \theta \leq 0 \\ l_0, & \text{for } \theta > 0. \end{cases} \tag{5}$$

The mechanical energy is restored and maximized as well as the angular momentum by moving the mass from A to E, as shown in Fig. 1, and restored value $\Delta E$ (in joules) yields

$$\Delta E = mg(l_1 - l_0)(1 - \cos\,\theta_0) \tag{6}$$

where $\theta_0$ (in radians) is the deviation angle when $\dot{\theta} = 0$ (at D and E positions). Lavrovskii and Formalskii [12] provide further details.

In the following, we discuss how we applied this pumping mechanism to controlling the swing leg of a planar telescopic legged biped robot.

## III. Modeling Planar Telescopic Legged Biped

This section describes the mathematical model for the simplest planar biped robot with telescopic legs.

### A. Dynamic Equation

This paper deals with a planar biped robot with telescopic legs, as shown in Fig. 2. We assumed that the robot did not have rotational actuators at the hip or ankle joints, and only had telescopic actuators on the legs. By moving the swing leg's mass in the leg direction following our proposed method, the robot system can increase the mechanical energy based on how effective parametric excitation is. We assumed that the stance leg's actuator would be mechanically locked during the stance

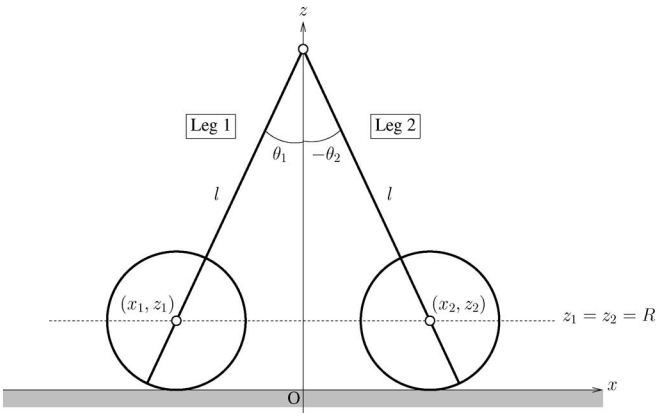


Fig. 3. Geometric relation at transition instant.

phase maintaining the length $b_1 = b$, where $b$ is constant. The length of the lower parts, i.e., $a_1$ and $a_2$, is equal to constant $a$. The swing leg length $b_2$ was also adjusted to the desired values before heel-strike impact. The robot can then be modeled as a 3-DOF system whose generalized coordinate vector is $\boldsymbol{q} = [\,\theta_1 \quad \theta_2 \quad b_2\,]^{\mathrm{T}}$, as shown in Fig. 2.

Several past researchers have considered the telescopic leg mechanism in PDW. Although van der Linde introduced it as a compliance mechanism [13] and Osuka and Saruta adopted it to avoid foot scuffing during the stance phase [14], its dynamics and effect on restoring mechanical energy have thus far not been investigated.

The dynamic equation is given by

$$\boldsymbol{M}(\boldsymbol{q})\ddot{\boldsymbol{q}} + \boldsymbol{h}(\boldsymbol{q}, \dot{\boldsymbol{q}}) = \boldsymbol{S}u \tag{7}$$

where $\boldsymbol{M}(\boldsymbol{q}) \in \mathbb{R}^{3\times 3}$ is the inertia matrix and $\boldsymbol{h}(\boldsymbol{q}, \dot{\boldsymbol{q}}) \in \mathbb{R}^3$ is the vector for Coriolis, centrifugal, and gravity forces. The variable $u$ is the control input for the telescopic actuator on the swing leg.

### B. Transition Equation

The positional state variables can be reset very easily. Assuming that the pumping of the swing leg has been controlled before heel-strike impact, i.e., the swing leg is as long as the stance leg (nominal length), the robot is symmetrical with respect to the $z$-axis, as shown in Fig. 3. The positional vector, $\boldsymbol{q}$, should be then reset as

$$\boldsymbol{q}^+ = \begin{bmatrix} 0 & 1 & 0 \\ 1 & 0 & 0 \\ 0 & 0 & 1 \end{bmatrix} \boldsymbol{q}^-. \tag{8}$$

The velocities, on the other hand, are reset according to the following algorithms by introducing the extended generalized coordinate vector, $\bar{\boldsymbol{q}} \in \mathbb{R}^6$. The heel-strike collision model can be modeled as

$$\bar{\boldsymbol{M}}(\bar{\boldsymbol{q}})\dot{\bar{\boldsymbol{q}}}^+ = \bar{\boldsymbol{M}}(\bar{\boldsymbol{q}})\dot{\bar{\boldsymbol{q}}}^- - \boldsymbol{J}_I(\bar{\boldsymbol{q}})^{\mathrm{T}}\boldsymbol{\lambda}_I \tag{9}$$

$$\boldsymbol{J}_I(\bar{\boldsymbol{q}})\dot{\bar{\boldsymbol{q}}}^+ = \boldsymbol{0}_{4\times 1} \tag{10}$$

where $\boldsymbol{J}_I(\bar{\boldsymbol{q}}) \in \mathbb{R}^{4\times 6}$ is the Jacobian matrix derived following the geometric condition at impact, $\boldsymbol{\lambda}_I \in R^4$ is the Lagrange's undetermined multiplier vector within the context of impulsive force, and (10) represents the velocity constraint conditions just after impact. The generalized coordinate vector in this case is defined as $\bar{\boldsymbol{q}} := [\,\bar{\boldsymbol{q}}_1^{\mathrm{T}} \quad \bar{\boldsymbol{q}}_2^{\mathrm{T}}\,]^{\mathrm{T}}$ and $\bar{\boldsymbol{q}}_i := [\,x_i \quad z_i \quad \theta_i\,]^{\mathrm{T}}$. The inertia matrix $\bar{\boldsymbol{M}}(\bar{\boldsymbol{q}}) \in \mathbb{R}^{6\times 6}$ is derived according to $\bar{\boldsymbol{q}}$ and detailed as

$$\bar{\boldsymbol{M}}(\bar{\boldsymbol{q}}) = \begin{bmatrix} \boldsymbol{M}_1(\bar{\boldsymbol{q}}_1) & \boldsymbol{0}_{3\times 3} \\ \boldsymbol{0}_{3\times 3} & \boldsymbol{M}_2(\bar{\boldsymbol{q}}_2) \end{bmatrix} \tag{11}$$

$$\boldsymbol{M}_i(\bar{\boldsymbol{q}}_i) = \begin{bmatrix} m & 0 & m(a-R)\cos\theta_i \\ & m & -m(a-R)\sin\theta_i \\ \mathrm{Sym} & & I + m(a-R)^2 \end{bmatrix}. \tag{12}$$

The matrix $\boldsymbol{M}_i(\bar{\boldsymbol{q}}_i) \in \mathbb{R}^{3\times 3}$ is the inertia matrix for leg $i$. Note $\bar{\boldsymbol{q}} = \bar{\boldsymbol{q}}^+ = \bar{\boldsymbol{q}}^-$ in (10), and impulsive force vector $\boldsymbol{\lambda}_I$ in (9) can be derived as

$$\boldsymbol{\lambda}_I\left(\bar{\boldsymbol{q}}, \dot{\bar{\boldsymbol{q}}}\right) = \boldsymbol{X}_I(\bar{\boldsymbol{q}})^{-1}\boldsymbol{J}_I(\bar{\boldsymbol{q}})\dot{\bar{\boldsymbol{q}}}^- \tag{13}$$

$$\boldsymbol{X}_I(\bar{\boldsymbol{q}}) = \boldsymbol{J}_I(\bar{\boldsymbol{q}})\bar{\boldsymbol{M}}(\bar{\boldsymbol{q}})^{-1}\boldsymbol{J}_I(\bar{\boldsymbol{q}})^{\mathrm{T}}. \tag{14}$$

By substituting (13) into (9), we obtain

$$\dot{\bar{\boldsymbol{q}}}^+ = \left(\boldsymbol{I}_6 - \boldsymbol{M}^{-1}\boldsymbol{J}_I^{\mathrm{T}}\boldsymbol{X}_I^{-1}\boldsymbol{J}_I\right)\dot{\bar{\boldsymbol{q}}}^-. \tag{15}$$

Note that $\dot{\bar{\boldsymbol{q}}}^-$ is given by transforming $\dot{\boldsymbol{q}}^-$ as

$$\dot{\bar{\boldsymbol{q}}}^- = \begin{bmatrix} R & 0 & 0 \\ 0 & 0 & 0 \\ 1 & 0 & 0 \\ R + (l-R)\cos\theta_1 & -(l-R)\cos\theta_2 & 0 \\ -(l-R)\sin\theta_1 & (l-R)\sin\theta_2 & 0 \\ 0 & 1 & 0 \end{bmatrix} \dot{\boldsymbol{q}}^- =: \boldsymbol{H}(\bar{\boldsymbol{q}})\dot{\boldsymbol{q}}^-. \tag{16}$$

However, assuming $\dot{b}_2^+ = 0$, the transformation from $\dot{\bar{\boldsymbol{q}}}^+$ to $\dot{\boldsymbol{q}}^+$ yields

$$\dot{\boldsymbol{q}}^+ = \begin{bmatrix} 0 & 0 & 0 & 0 & 0 & 1 \\ 0 & 0 & 1 & 0 & 0 & 0 \\ 0 & 0 & 0 & 0 & 0 & 0 \end{bmatrix} \dot{\bar{\boldsymbol{q}}}^+. \tag{17}$$

We can then compute $\dot{\boldsymbol{q}}^+$ from $\dot{\boldsymbol{q}}^-$ by following (15)–(17).

### C. Mechanical Energy

The total mechanical energy $E$ (in joules) is defined by the sum of kinetic and potential energy as

$$E(\boldsymbol{q}, \dot{\boldsymbol{q}}) = \frac{1}{2}\dot{\boldsymbol{q}}^{\mathrm{T}}\boldsymbol{M}(\boldsymbol{q})\dot{\boldsymbol{q}} + P(\boldsymbol{q}) \tag{18}$$

and its time derivative satisfies the relation $\dot{E} = \dot{\boldsymbol{q}}^{\mathrm{T}}\boldsymbol{S}\boldsymbol{u} = \dot{b}_2 u$. It remains constant with zero input, or PDW on a gentle slope. It should be steadily increased during the stance phase on level ground to restore the lost energy by every heel-strike collisions.

## IV. Parametrically Excited Dynamic Bipedal Walking

This section proposes a simple law to control telescopic leg actuation and investigates a typical dynamic gait produced by the effect of parametric excitation.

### A. Control Law

A level gait can be generated by simply controlling pumping to the swing leg. We propose output following control in this paper to reproduce the parametric excitation mechanism in Fig. 1 by expanding and contracting the swing leg length. We chose the telescopic length of the swing leg, $b_2 = \boldsymbol{S}^{\mathrm{T}}\boldsymbol{q}$, as the system's output, and its second-order derivative yields

$$\ddot{b}_2 = \boldsymbol{S}^{\mathrm{T}}\boldsymbol{M}^{-1}\boldsymbol{S}u - \boldsymbol{S}^{\mathrm{T}}\boldsymbol{M}^{-1}\boldsymbol{h}. \tag{19}$$

Let $b_{2\mathrm{d}}(t)$ be the time-dependent trajectory for $b_2$, and the control input that exactly achieves $b_2 \equiv b_{2\mathrm{d}}(t)$ can be determined as

$$u = \left(\boldsymbol{S}^{\mathrm{T}}\boldsymbol{M}^{-1}\boldsymbol{S}\right)^{-1}\left(\ddot{b}_{2\mathrm{d}} + \boldsymbol{S}^{\mathrm{T}}\boldsymbol{M}^{-1}\boldsymbol{h}\right). \tag{20}$$

This paper gives the control input in (20) as a continuous-time signal to enable the exact gait to be evaluated. Considering smooth pumping motion, we intuitively introduced a time-dependent trajectory $b_{2\mathrm{d}}(t)$ to enable telescopic leg motion

$$b_{2\mathrm{d}}(t) = \begin{cases} b - A\sin^3\left(\frac{\pi}{T_{\mathrm{set}}}t\right), & \text{for } t \le T_{\mathrm{set}} \\ b, & \text{for } t > T_{\mathrm{set}} \end{cases} \tag{21}$$

where $T_{\mathrm{set}}$ (in seconds) is the desired settling time, and where we assumed that $T_{\mathrm{set}}$ would occur before heel-strike collisions. In other words, let $T$ (in seconds) be the steady-step period, and condition $T \ge T_{\mathrm{set}}$ should always hold. We called this the settling time condition. Since $\ddot{b}_{2\mathrm{d}}(T_{\mathrm{set}})$ is not differentiable but continuous here, the control input $u$ also becomes continuous.

### B. Numerical Simulations

Fig. 4 shows the simulation results for parametrically excited dynamic bipedal walking where $A = 0.08$ m and $T_{\mathrm{set}} = 0.55$ s. The same physical parameters were chosen as in Table 1. Fig. 5 shows one cycle of motion of the walking pattern. We can see from the results that a stable limit cycle is generated by the effect of the proposed method. We can see from Fig. 4(b) and (c) that the leg length is successfully controlled and settled to the desired length $b$ (in meters) before all heel-strike collisions whereas the mechanical energy is restored by the effect of parametric excitation. Stable dynamic biped level locomotion can be easily achieved without taking the ZMP condition into account since this robot does not use (or require) ankle joint torque. The ZMP in this case is identical to the contact point of the sole with the ground, and travels forward monotonically from the heel to the tiptoe assuming that condition $\dot{\theta}_1 \ge 0$ holds. This property appears human-like.

As seen in Fig. 4(a), the mechanical energy is not restored monotonically but lost by expanding the swing leg. It is necessary to monotonically restore mechanical energy to obtain maximum efficiency [8], and how to improve this will be investigated in Section V. Before discussing this, in the next section, we will discuss the gait efficiency according to several system parameters in detail.

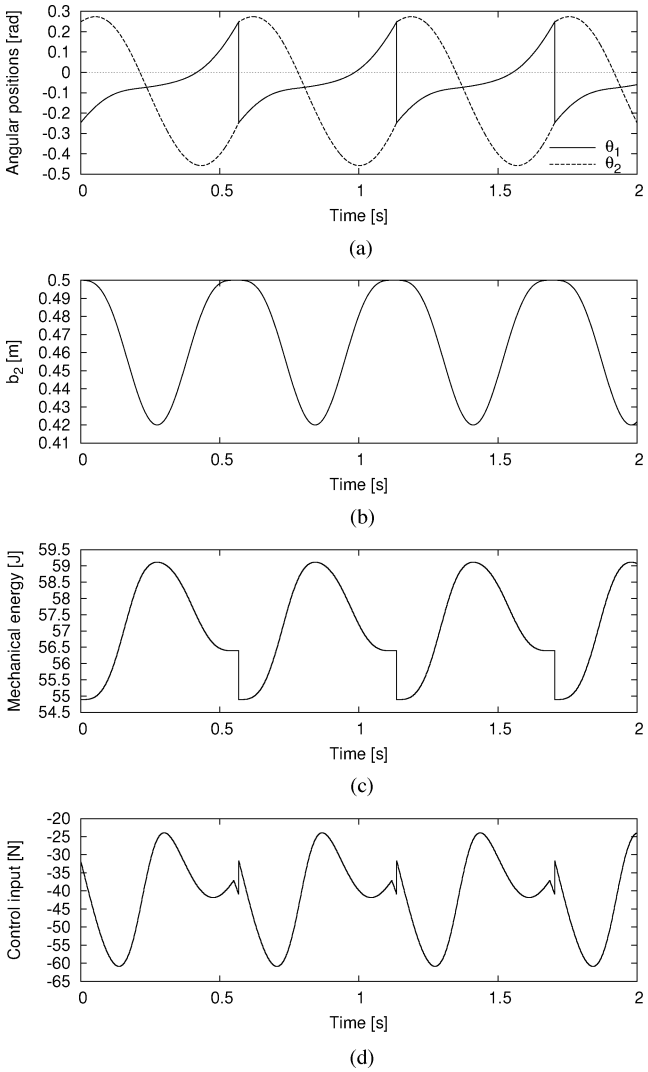


Fig. 4. Simulation results for parametrically excited dynamic bipedal walking, where $A = 0.08$ m and $T_{\mathrm{set}} = 0.55$ s. (a) Angular position. (b) $b_2$. (c) Mechanical energy. (d) Control input.

TABLE I
PHYSICAL PARAMETER SETTINGS FOR BIPED ROBOT

| | | |
|---|---|---|
| $a\ (= a_1 = a_2)$ | 0.5 | m |
| $b\ (= b_1)$ | 0.5 | m |
| $R$ | 0.5 | m |
| $m$ | 5.0 | kg |
| $I$ | 0.1 | kg·m$^2$ |

## V. PARAMETER STUDY

This section discusses our analysis of changes in gait according to control parameters and the foot radius.

### A. Performance Indexes

Let us introduce criterion functions before performing numerical analysis. Let $T$ (in seconds) be the steady-step period. For simplicity, every just after impact (or start) time has been denoted in the following sections as $t = 0^+$ and every just before impact time of the next heel strike as $T^-$ by resetting the absolute time at every transition instant. Thus, $T^+$ means the

Fig. 5. One cycle of motion for parametrically excited dynamic bipedal walking in Fig. 4.

same as $0^+$. The average walking speed $v$ (in meters per second) is then defined as

$$v := \frac{1}{T}\int_{0^+}^{T^-} \dot{x}_{\rm G}\ {\rm d}t = \frac{\Delta x_{\rm G}}{T} \tag{22}$$

where $x_{\rm G}$ (in meters) is the $x$-position at the center of gravity and $\Delta x_{\rm G} := x_{\rm G}(T^-) - x_{\rm G}(0^+)$ (in meters). The average input power $p$ (in joules per second) is also defined as

$$p := \frac{1}{T}\int_{0^+}^{T^-} \left|\dot{b}_2 u\right| {\rm d}t. \tag{23}$$

Energy efficiency is then evaluated by specific resistance $p/Mgv$, which means the expenditure of energy per unit mass and per unit length, and this is a dimensionless quantity [7], [8]. The main question of how to attain energy-efficient biped locomotion rests on how to increase walking speed $v$ while keeping $p$ small. Restored mechanical energy, on the other hand, is also an important index for generating gait because whether it is positive or not indicates the generation of a stable limit cycle. This is determined as $\Delta E := E(T^-) - E(0^+)$ (in joules), and it should be positive if a stable gait is generated.

### B. Effect of Settling Time $T_{\rm set}$

Let us first examine the effect of the desired settling time $T_{\rm set}$. Fig. 6 shows the analysis results of the gait descriptors for three values of $A$. Here, (a) is the step period, (b) the walking speed, (c) the specific resistance, and (d) the restored mechanical energy. As previously mentioned, the settling time condition must be satisfied as an indicator of limit cycle generation, and this is strongly supported by Fig. 6(a); the $45^\circ$ line indicates the limit of settling time $T_{\rm set} = T$. We can see that the gait efficiency, walking speed, and specific resistance monotonically worsen with the decrease in $T_{\rm set}$. This is because telescopic leg actuation cannot cause sufficient parametric excitation effect within a short time. From Fig. 6(d), we can also see that hardly no mechanical energy is restored during steps with a short pumping time. The timing for pumping the leg must synchronize with the mechanism for parametric excitation, and short $T_{\rm set}$ generally cannot achieve this.

### C. Effect of Leg Mass Position $a$

Next, the nominal leg mass position $a$, or the length from the tiptoe to CoM, is adjusted while maintaining $a + b = l = 1.0$ m. Fig. 7 shows the analysis results of the gait descriptors for three values of $A$ where $T_{\rm set} = 0.55$ s. In all cases in Fig. 7(b) and (c), there is an optimal $a$ that yields a maximum walking speed and a minimum specific resistance. Fig. 7(a) also shows that the settling time condition is always satisfied. With large pumping amplitude $A$, as seen in Fig. 7(d), there is a great deal of parametric excitation, and consequently, much mechanical energy is restored. This promotes leg-swing motion and the step period then lengthens as shown in Fig. 7(a). As $a$ increases, the pendulum in Fig. 1 shortens, and the mechanism for parametric excitation becomes hard to effect. This is confirmed by the restored mechanical energy in Fig. 7(d).

### D. Effect of Foot Radius $R$

As Tedrake *et al.* [15] and Wisse *et al.* [16] pointed out, adjusting foot radius $R$ can effectively improve the walking system's efficiency. The robot can engage in high-speed level walking without having to change the control law with a suitable choice of $R$. Fig. 8 shows the analysis results of the gait descriptors for three values of $A$ where $T_{\rm set} = 0.55$ s. We can see that the step period in each case monotonically decreases with the increase in $R$, and there is an optimal $R$ that yields the best gait efficiency in terms of the maximum walking speed and minimum specific resistance. The walking speeds thus obtained are remarkably faster than those with previous major approaches inspired by PDW with ankle joint actuation using flat-footed models [8], [17].

Parametrically excited gaits often exhibit period-doubling bifurcation and chaotic motion as do the original passive dynamic gait without any actuation [18]–[20] and virtual PDW on level ground [8]. The walking system has a tendency to exhibit period-doubling bifurcation as $R$ becomes small in each case, as seen from the results. Small $R$ has less of an effect on propelling the walking system forward based on parametric excitation, whereas large $R$ also leads to the same results. The optimal value must be found numerically.

Although the importance of foot radius $R$ has been empirically known, no theoretical studies have yet been done. The foot radius can be the main adjustment parameter to improve gait efficiency, and it should be investigated in more detail to accomplish truly energy-efficient and high-speed dynamic biped locomotion. We will investigate the mechanism in more detail in Section VI.

## VI. Improvements in Energy Efficiency Using Elastic Element

Since the pumping motion of swing leg causes energy loss, as mentioned in Section III, it leads to inefficient walking. This section therefore investigates improved energy efficiency achieved by using an elastic element and adjusting its mechanical impedances.

### A. Model With Elastic Elements

Telescopic leg actuation requires very large force to raise the entire leg mass and this causes inefficient dynamic walking. The utilization of elastic elements should be considered to solve this problem. This section introduces a model with elastic elements, and we analyze its effectiveness through numerical simulations.

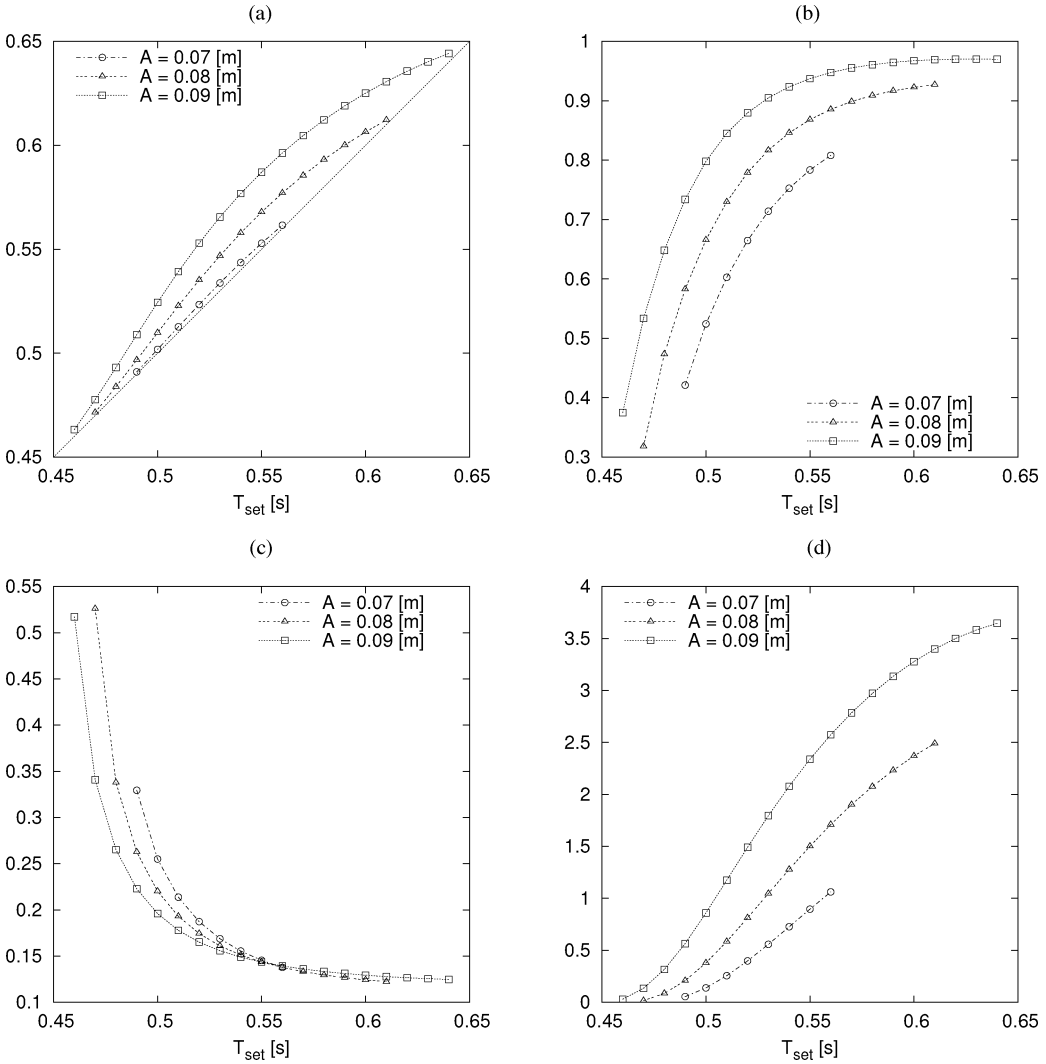


Fig. 6. Gait descriptors with respect to $T_{\rm set}$ for three values of $A$ where $a = b = 0.50$ m. (a) Step period (in seconds). (b) Walking speed (in meters per second). (c) Specific resistance. (d) Restored mechanical energy (in joules).

Fig. 9 outlines a biped model with elastic elements where $k > 0$ (in newtons per meter) is the elastic coefficient and $b_0$ (in meters) is the nominal length. Its dynamic equation during the swing phase is given by

$$\boldsymbol{M}(\boldsymbol{q})\ddot{\boldsymbol{q}} + \boldsymbol{h}(\boldsymbol{q}, \dot{\boldsymbol{q}}) = \boldsymbol{S}u - \frac{\partial Q(\boldsymbol{q})}{\partial \boldsymbol{q}^{\rm T}} \tag{24}$$

where $Q$ (in joules) is the elastic energy defined as

$$Q(\boldsymbol{q}) := \frac{1}{2}k\left(b_2 - b_0\right)^2. \tag{25}$$

The other terms except for the elastic effect are the same as those in (7).

We here redefine the total mechanical energy including the elastic energy $Q$ as

$$E(\boldsymbol{q}, \dot{\boldsymbol{q}}) := \frac{1}{2}\dot{\boldsymbol{q}}^{\rm T}\boldsymbol{M}(\boldsymbol{q})\dot{\boldsymbol{q}} + P(\boldsymbol{q}) + Q(\boldsymbol{q}) \tag{26}$$

and its time derivative yields

$$\dot{E} = \dot{b}_2 u. \tag{27}$$

### B. Efficiency Analysis

The control input $u$ to exactly achieve $b_2 \equiv b_{2\rm d}$ in this case is determined to cancel out the elastic effect in (24) as

$$u = \left(\boldsymbol{S}^{\rm T}\boldsymbol{M}^{-1}\boldsymbol{S}\right)^{-1}\left(\ddot{b}_{2\rm d} + \boldsymbol{S}^{\rm T}\boldsymbol{M}^{-1}\left(\boldsymbol{h} + \frac{\partial Q}{\partial \boldsymbol{q}^{\rm T}}\right)\right). \tag{28}$$

This does not change walking motion regardless of the elastic element's mechanical impedances. Only the actuator's burden is adjusted. The maximum energy-efficiency condition is then found by the combination of $k$ and $b_0$ that minimize the average input power $p$. The following relation holds for the definite integral of the absolute function to

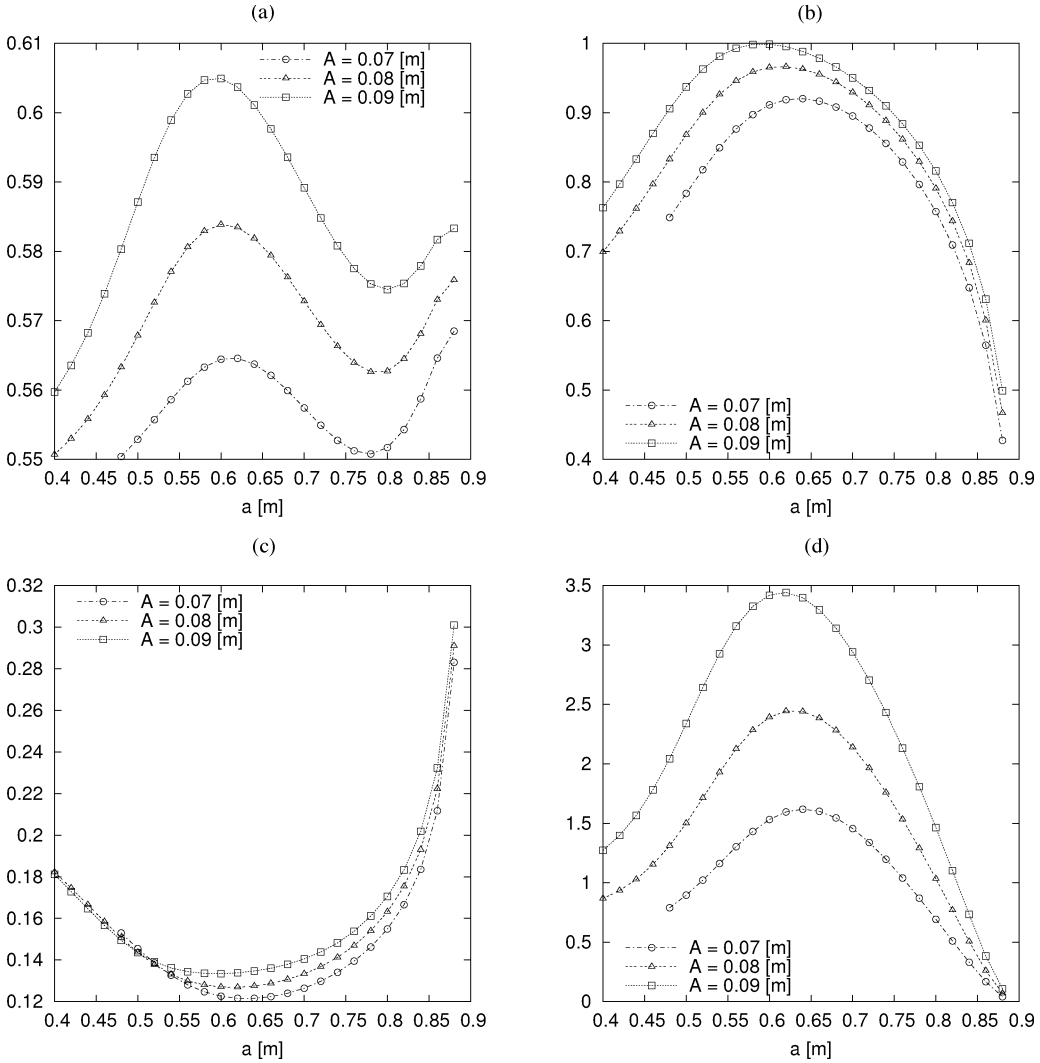


Fig. 7. Gait descriptors with respect to $a$ for three values of $A$ where $T_{\rm set} = 0.55$ s. (a) Step period (in seconds). (b) Walking speed (in meters per second). (c) Specific resistance. (d) Restored mechanical energy (in joules).

calculate $p$:

$$p \geq \frac{1}{T}\int_{0^+}^{T^-} \dot{b}_2 u \, \mathrm{d}t = \frac{1}{T}\int_{0^+}^{T^-} \dot{E} \, \mathrm{d}t = \frac{\Delta E}{T}. \qquad (29)$$

Therefore, following (22) and (29), we can obtain the relation

$$\frac{p}{Mgv} \geq \frac{\Delta E}{Mg\Delta x_{\rm G}}. \qquad (30)$$

Here, note that the equality holds in (29) if and only if $\dot{E} = \dot{b}_2 u \geq 0$. This means that the monotonic restoration of mechanical energy by control input is the necessary condition for maximum efficiency [8].

Fig. 10 shows the specific resistance with respect to $k$ and $b_0$ with its contours. There is an optimal combination of $k$ and $b_0$ in the valley of the 3-D plot, and the specific resistance is kept quite small at less than $0.04$, which is much smaller than that of previous major works. The gait obtained with optimal mechanical impedances is much faster than that with virtual PDW at the same value for specific resistance. Fig. 11 plots the time evolutions of the total mechanical energy for six values of $k$ where $b_0 = 0.30$ m. In this case, $k = 225$ N/m provides the best efficiency, and the figure gives the proof; energy is almost monotonically restored when $k = 225$ N/m. Fig. 12 plots the time evolutions of the total mechanical energy for six values of $b_0$ (in meters) where $k = 225$ N/m. Here, $b_0 = 0.30$ m yields the best performance, which the figure shows.

The edges of the 3-D plot in Fig. 10 are lines where $k = 0$ and $b_0 = 0.46$ with the same value. The specific resistance where $k = 0$ is of course kept constant, regardless of $b_0$, i.e., the value without any power assist. On the other hand, $b_0 = 0.46$ m, which is equivalent to $b - A/2$, yields the same efficiency as in the case of $k = 0$ regardless of $k$. This can be explained as follows. Equation (28) can be expressed as

$$u = u_0 + k(b_2 - b_0) \qquad (31)$$

where $u_0$ is the same as $u$ in (20). The sign of $u$ is always negative when $b_0 = b - A/2$, and thus, that of $\dot{E} = \dot{b}_2 u$ is equivalent to that of $-\dot{b}_2$. The input power integral can then be divided as

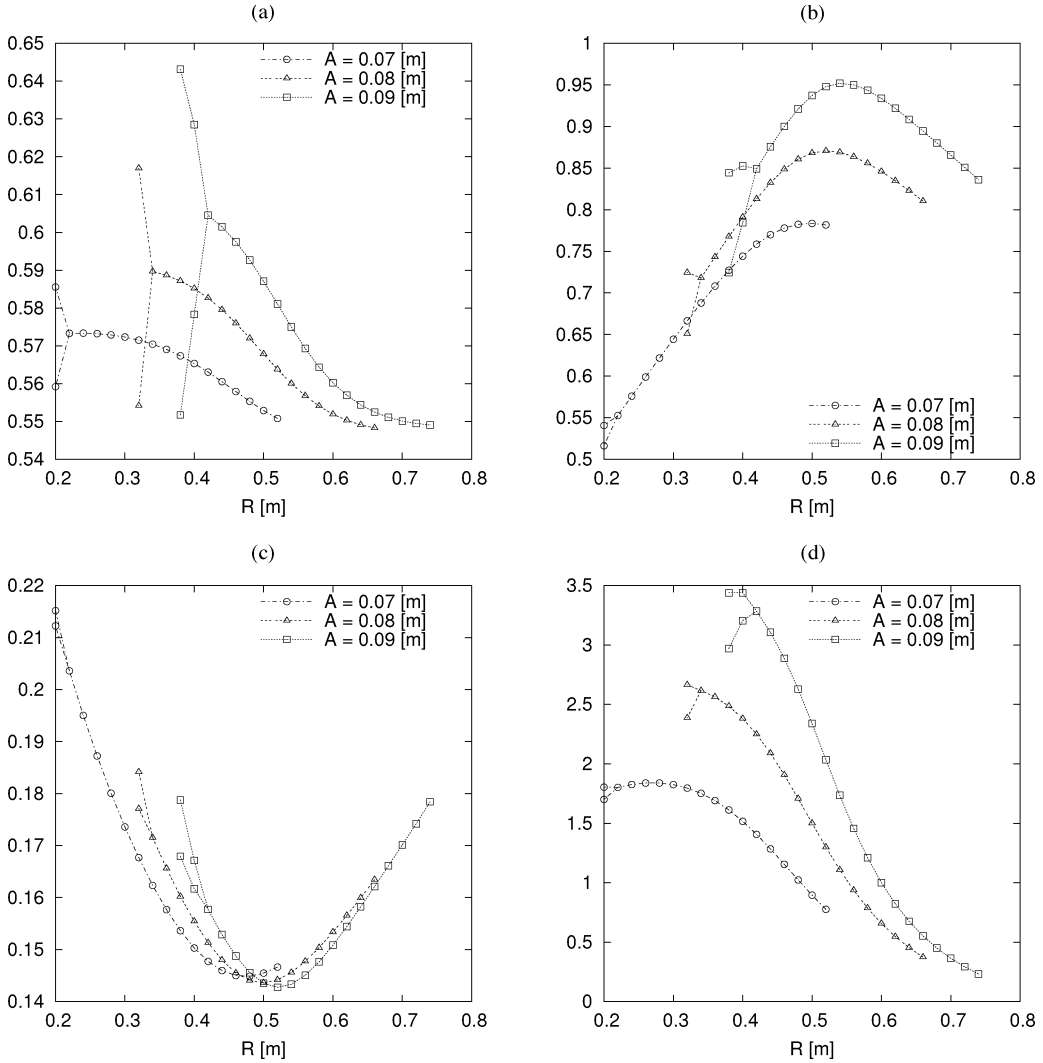


Fig. 8. Gait descriptors with respect to $R$ for three values of $A$, where $T_{\rm set} = 0.55$ s, and $a = b = 0.50$ m. In each case, period-doubling bifurcation occurs when $R$ is small. (a) Step period (in seconds). (b) Walking speed (in meters per second). (c) Specific resistance. (d) Restored mechanical energy (in joules).

follows:

$$\begin{aligned}\int_{0^+}^{T^-} \left|\dot{b}_2 u\right| \mathrm{d}t &= \int_{0^+}^{T_{\rm set}/2} \dot{b}_2 u \, \mathrm{d}t - \int_{T_{\rm set}/2}^{T_{\rm set}} \dot{b}_2 u \, \mathrm{d}t \\ &= \int_{0^+}^{T_{\rm set}/2} \dot{b}_2 \left(u_0 + k(b_2 - b_0)\right) \mathrm{d}t \\ &\quad - \int_{T_{\rm set}/2}^{T_{\rm set}} \dot{b}_2 \left(u_0 + k(b_2 - b_0)\right) \mathrm{d}t \quad (32)\end{aligned}$$

Here, the following relations hold:

$$\int_{0^+}^{T_{\rm set}/2} k\dot{b}_2(b_2 - b_0)\mathrm{d}t = \left[\frac{1}{2}k(b_2 - b_0)^2\right]_{b_2 = b_0 + (A/2)}^{b_2 = b_0 - (A/2)} = 0$$

$$\int_{T_{\rm set}/2}^{T_{\rm set}} k\dot{b}_2(b_2 - b_0)\mathrm{d}t = \left[\frac{1}{2}k(b_2 - b_0)^2\right]_{b_2 = b_0 - (A/2)}^{b_2 = b_0 + (A/2)} = 0.$$

Therefore, we can see that in this case, the term for elastic effect does not influence the energy efficiency at all. We should choose a $b_0$ of less than $b - A/2$ to ensure efficiency is improved.

Table II lists several values of specific resistance in related studies on limit cycle walkers. The value of human is also added for the purpose of reference and is measured in a different way than others. The variable $\phi$ (in radians) is the (virtual) slope angle for (virtual) PDW. We can confirm that parametrically excited walking with elasticity achieves sufficiently small value compared with others. It is also important to remember that virtual PDW achieves small value in accordance with the virtual slope angle.

## VII. Effect of Foot Radius $R$ on Heel-Strike Collisions

As seen in Section IV, the rolling effect of semicircular feet on the walking speed is noteworthy. This section discusses the effect of the foot radius $R$ on heel-strike collisions.

### A. Dissipated Mechanical Energy

The total mechanical energy dissipated by heel-strike collision $\Delta E_{\rm hs}$ is equivalent to the dissipated kinetic energy and is

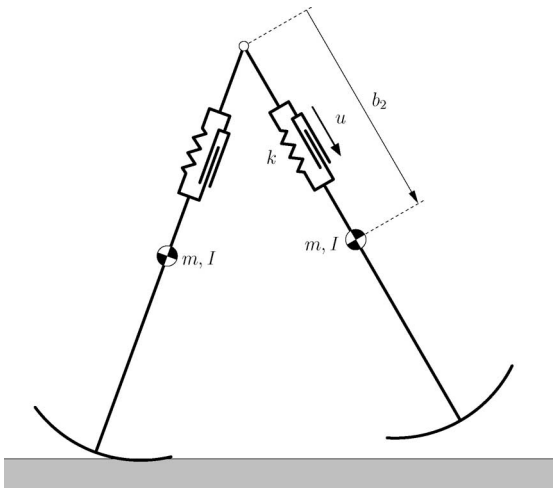


Fig. 9. Model of planar telescopic legged biped with elastic elements.

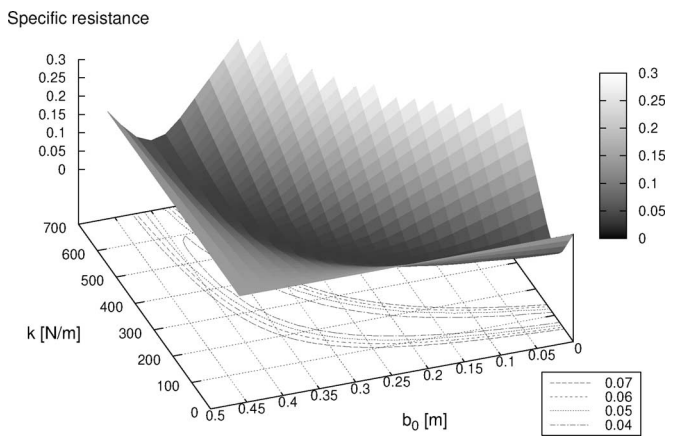


Fig. 10. Specific resistance with respect to elastic coefficient $k$ and natural length $b_0$ and its contours. Minimum value is about 0.031.

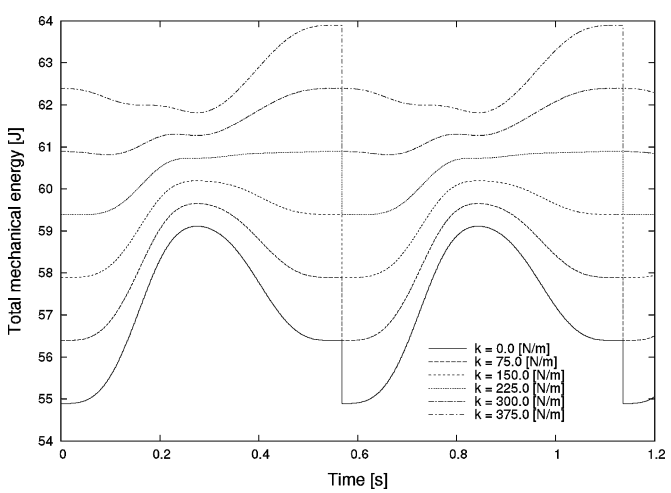


Fig. 11. Time evolution of total mechanical energy for six values of $k$.

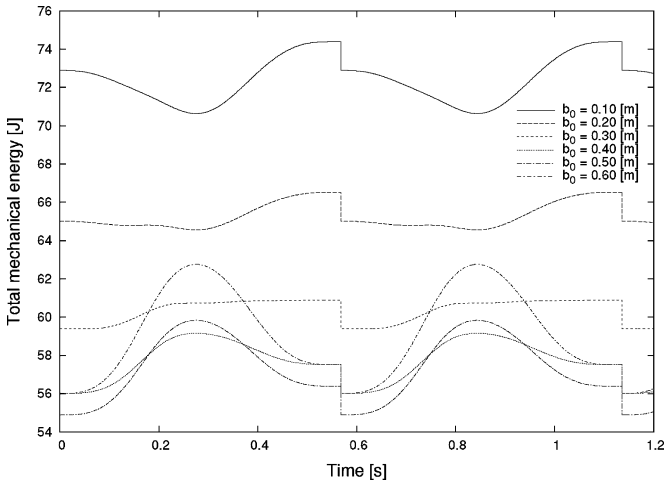


Fig. 12. Time evolution of total mechanical energy for six values of $b_0$.

TABLE II
COMPARISON OF ENERGY EFFICIENCY

| Type of dynamic walker | Specific resistance [-] |
|---|---|
| Human | 0.05 |
| Honda's Asimo | 1.6 |
| Cornell biped [7] | 0.055 |
| Passive dynamic walking [6] | $\sin\phi$ ($\phi = 0.005 \sim 0.09$) |
| Virtual passive dynamic walking [8] | $\tan\phi$ ($\phi = 0.005 \sim 0.09$) |
| Parametric excitation without elasticy | 0.12 |
| Parametric excitation with elasticy | 0.031 |

expressed as

$$\Delta E_{\rm hs} := \frac{1}{2}(\dot{\bar{\boldsymbol{q}}}^+)^{\rm T}\bar{\boldsymbol{M}}(\bar{\boldsymbol{q}})\dot{\bar{\boldsymbol{q}}}^+ - \frac{1}{2}(\dot{\bar{\boldsymbol{q}}}^-)^{\rm T}\bar{\boldsymbol{M}}(\bar{\boldsymbol{q}})\dot{\bar{\boldsymbol{q}}}^- \leq 0. \quad (33)$$

By substituting (15) into (33) and eliminating $\dot{\bar{\boldsymbol{q}}}^+$, we can arrange $\Delta E_{\rm hs}$ as follows:

$$\Delta E_{\rm hs} = -\frac{1}{2}(\dot{\bar{\boldsymbol{q}}}^-)^{\rm T}\boldsymbol{J}_I^{\rm T}\boldsymbol{X}_I^{-1}\boldsymbol{J}_I\dot{\bar{\boldsymbol{q}}}^-. \quad (34)$$

Further, by considering (16), this yields

$$\Delta E_{\rm hs} = -\frac{1}{2}(\dot{\boldsymbol{q}}^-)^{\rm T}\boldsymbol{H}^{\rm T}\boldsymbol{J}_I^{\rm T}\boldsymbol{X}_I^{-1}\boldsymbol{J}_I\boldsymbol{H}\dot{\boldsymbol{q}}^-. \quad (35)$$

Here, note that $\boldsymbol{H}$, $\boldsymbol{J}_I$, and $\boldsymbol{X}_I$ are only function matrices of $\theta_i$. Let $\alpha$ (in radians) be the absolute value of the half interleg angle at the transition instant. The angular positions in Fig. 3 can then be expressed as $\theta_1 = \alpha$ and $\theta_2 = -\alpha$. The following matrix $\boldsymbol{N} \in \mathbb{R}^{3\times 3}$

$$\boldsymbol{N} := \boldsymbol{H}^{\rm T}\boldsymbol{J}_I^{\rm T}\boldsymbol{X}_I^{-1}\boldsymbol{J}_I\boldsymbol{H} \quad (36)$$

only becomes a function matrix of $\alpha$. The dissipated kinetic energy finally yields

$$\Delta E_{\rm hs} = -\frac{1}{2}(\dot{\boldsymbol{q}}^-)^{\rm T}\boldsymbol{N}(\alpha)\dot{\boldsymbol{q}}^-. \quad (37)$$

We treat matrix $\boldsymbol{N}$ as a function matrix of $R$ and $\alpha$ in the following.

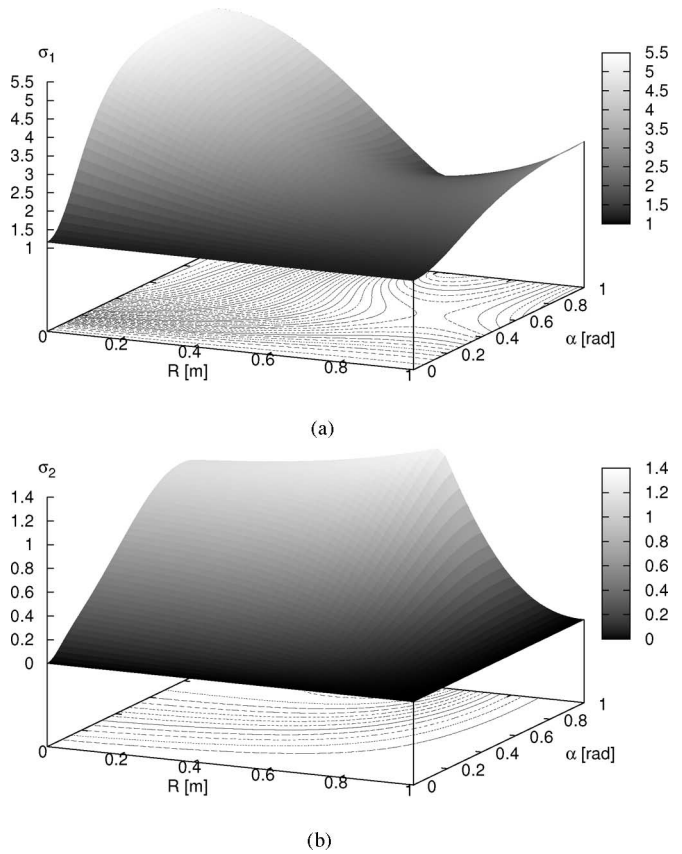


Fig. 13. Singular values of matrix $\boldsymbol{N}$ and their contours with respect to $R$ and $\alpha$. (a) $\sigma_1$. (b) $\sigma_2$.

### B. Analysis Based on Singular Value

It is very difficult to analytically analyze the detailed structure of $\Delta E_{\rm hs}$. One candidate for evaluating the dissipative feature is the singular value of $\boldsymbol{N}$. Note that $\boldsymbol{N}$ is always positive semidefinite, or singular because the state variable $b_2$, whose time derivative is assumed to be 0 at just before and after impact, is not related to the collision dynamics. Therefore, $\boldsymbol{N}$ always has a minimum singular value of 0, regardless of other physical parameters, and the singular value decomposition (SVD) of matrix $\boldsymbol{N}$ has the form

$$\boldsymbol{N} = \boldsymbol{V}\boldsymbol{\Sigma}\boldsymbol{V}^{\rm T}, \qquad \boldsymbol{\Sigma} = \begin{bmatrix} \sigma_1 & 0 & 0 \\ 0 & \sigma_2 & 0 \\ 0 & 0 & 0 \end{bmatrix} \tag{38}$$

where $\sigma_1 \geq \sigma_2 \geq 0$ and $\boldsymbol{V} \in \mathbb{R}^{3\times 3}$ is a unitary matrix. Fig. 13(a) and (b) shows $\sigma_1$ and $\sigma_2$ of matrix $\boldsymbol{N}$ and their contours with respect to $R$ and $\alpha$ where the physical parameters are those chosen from Table 1. The maximum singular value $\sigma_1$ implies the worst case of energy dissipation. As the contour in Fig. 13(a) strongly indicates, an optimal choice of $R$ that minimizes $\sigma_1$ can be found for the given $\alpha$. Note that $\sigma_2$ is 0 when $R = l$ or $\alpha = 0$, as seen in Fig. 13(b). This means that there is a solution, i.e., $\dot{\boldsymbol{q}}^- \neq \boldsymbol{0}_{3\times 1}$, to achieve $\Delta E_{\rm hs} = 0$ in these cases. Let us derive its condition in the following:

where $R = l$, and matrix $\boldsymbol{N}$ has the form

$$\boldsymbol{N} = N_{R=l}\begin{bmatrix} 1 & -1 & 0 \\ -1 & 1 & 0 \\ 0 & 0 & 0 \end{bmatrix} \qquad \boldsymbol{\Sigma} = \begin{bmatrix} \sigma_1 & 0 & 0 \\ 0 & 0 & 0 \\ 0 & 0 & 0 \end{bmatrix}$$
$$\boldsymbol{V} = \begin{bmatrix} -1/\sqrt{2} & -1/\sqrt{2} & 0 \\ 1/\sqrt{2} & -1/\sqrt{2} & 0 \\ 0 & 0 & 1 \end{bmatrix} \tag{39}$$

where

$$N_{R=l} = \frac{N_1}{N_2} > 0 \tag{40}$$

$$\begin{aligned} N_1 &= 2mR^2\left(I + m(a-R)^2\right) \\ &\quad \times \left(2I + m(a-R)^2(1-\cos(2\alpha))\right) \end{aligned} \tag{41}$$

$$\begin{aligned} N_2 &= 2I^2 + 4Ima^2 + 2m^2a^4 - 8ImaR - 8m^2a^3R \\ &\quad + 8ImR^2 + 15m^2a^2R^2 - 14m^2aR^3 + 5m^2R^4 \\ &\quad + 4m\left(I + m(a-R)^2\right)(a-R)R\cos\alpha \\ &\quad - m^2R^2(a-R)^2\cos(2\alpha). \end{aligned} \tag{42}$$

We can then solve the condition for $\Delta E_{\rm hs} = 0$. Let $\|\cdot\|$ be a vector norm, and substituting (39) into (37) gives

$$\begin{aligned} \Delta E_{\rm hs} &= -\frac{1}{2}\left\|\boldsymbol{\Sigma}^{1/2}\boldsymbol{V}^{\rm T}\dot{\boldsymbol{q}}^-\right\|^2 \\ &= -\frac{1}{2}\left\|\begin{bmatrix} \sqrt{\sigma_1} & 0 & 0 \\ 0 & 0 & 0 \\ 0 & 0 & 0 \end{bmatrix}\begin{bmatrix} -\frac{1}{\sqrt{2}} & \frac{1}{\sqrt{2}} & 0 \\ -\frac{1}{\sqrt{2}} & -\frac{1}{\sqrt{2}} & 0 \\ 0 & 0 & 1 \end{bmatrix}\begin{bmatrix} \dot{\theta}_1^- \\ \dot{\theta}_2^- \\ \dot{b}_2^- \end{bmatrix}\right\|^2 \\ &= -\frac{1}{4}\sigma_1\left(\dot{\theta}_1^- - \dot{\theta}_2^-\right)^2. \end{aligned} \tag{43}$$

Here, note that $\Delta E_{\rm hs}$ can also be derived following (37) as

$$\Delta E_{\rm hs} = -\frac{1}{2}N_{R=l}\left(\dot{\theta}_1^- - \dot{\theta}_2^-\right)^2 \tag{44}$$

and $2N_{R=l} = \sigma_1$ can be found. From (43) and (44), we can conclude that the energy dissipation is 0 when $\dot{\theta}_1^- = \dot{\theta}_2^-$; the energy dissipation can be reduced to zero by controlling the relative angular velocity just before impact of the hip joint, 0 rad/s, regardless of the choice of physical parameters.

McGeer studied this topic in his original work in 1990 [6], introducing a "synthetic wheel" with a massless leg. He pointed out that a synthetic wheel can walk on level ground without any power supply by choosing $R = l$ because support by the stance leg can roll seamlessly from one rim to the next. In addition, he remarked that the wheel should have a large point mass at the hip position, otherwise the swing leg motion would disrupt steady rolling. This is strongly supported by (41) because $\boldsymbol{N}$ becomes a zero matrix if $m = 0$. As our biped model has leg mass, it cannot behave as a synthetic wheel. Parametrically excited dynamic bipedal walking differs in nature from the wheel motion, and is only possible when there is leg mass.

Where $\alpha = 0$, matrix $\boldsymbol{N}$ can also be simplified and has form

$$\boldsymbol{N} = N_{\alpha=0} \begin{bmatrix} 1 & -1 & 0 \\ -1 & 1 & 0 \\ 0 & 0 & 0 \end{bmatrix} \tag{45}$$

where

$$N_{\alpha=0} = \frac{2Iml^2\left(I + mb^2\right)}{I^2 + 2Im\left(a^2 - al + l^2\right) + m^2a^2b^2} > 0. \tag{46}$$

Since matrix $\boldsymbol{N}$ has the same form as $R = l$ in this case, the condition for $\Delta E_{\rm hs} = 0$ is $\dot{\theta}_1^- = \dot{\theta}_2^-$. Condition $\alpha = 0$ seems unrealistic and is not considered to be a suitable transition posture to generate a stable limit cycle.

There is an optimal foot radius for minimizing the maximum singular value of $\boldsymbol{N}$, but we must find it numerically according to the robot's physical parameters or the shape at the transition instant. As we have seen in Section IV, parametrically excited dynamic bipedal walking requires sufficient magnitude for the foot radius to generate a stable limit cycle. We should conclude that a suitable foot radius would reduce energy dissipation, and as a result, this would lead to energy-efficient and high-speed dynamic biped locomotion together with parametric excitation. Constructing an optimal method of designing the shape of the foot is a subject for future study.

## VIII. Stability Analysis

This section investigates stability of the limit cycles. One way to analyze the orbital stability is the method of Poincaré return map [19]. As a natural choice of the discrete state $\boldsymbol{x}_k$ for the Poincaré section, we can take the state variables at instant of heel strikes, relative hip-joint angle, and angular velocities just after impact. $\boldsymbol{x}_k \in \mathbb{R}^3$ is then chosen as

$$\boldsymbol{x}_k = \begin{bmatrix} \theta_2^+[k] - \theta_1^+[k] \\ \dot{\theta}_1^+[k] \\ \dot{\theta}_2^+[k] \end{bmatrix} \tag{47}$$

where $k$ means the number of steps. The Poincaré return map can be denoted by a nonlinear discrete function $\boldsymbol{F}$ as

$$\boldsymbol{x}_{k+1} = \boldsymbol{F}(\boldsymbol{x}_k) \tag{48}$$

and the relation

$$\boldsymbol{x}^* = \boldsymbol{F}(\boldsymbol{x}^*) \tag{49}$$

holds in a steady gait where $\boldsymbol{x}^* \in \mathbb{R}^3$ is the stable equilibrium point for $\boldsymbol{x}_k$. Taylor series expansion of $\boldsymbol{F}$ around $\boldsymbol{x}^*$ yields

$$\begin{aligned} \boldsymbol{x}_{k+1} &= \boldsymbol{x}^* + \delta\boldsymbol{x}_{k+1} \\ &= \boldsymbol{F}(\boldsymbol{x}_k) \\ &= \boldsymbol{F}(\boldsymbol{x}^* + \delta\boldsymbol{x}_k) \\ &\approx \boldsymbol{F}(\boldsymbol{x}^*) + (\nabla\boldsymbol{F})\,\delta\boldsymbol{x}_k \end{aligned} \tag{50}$$

where $\nabla\boldsymbol{F}$ is the gradient of $\boldsymbol{F}$ with respect to the equilibrium point $\boldsymbol{x}^*$. Following (49) and (50), the discrete walking system yields

$$\delta\boldsymbol{x}_{k+1} = (\nabla\boldsymbol{F})\,\delta\boldsymbol{x}_k. \tag{51}$$

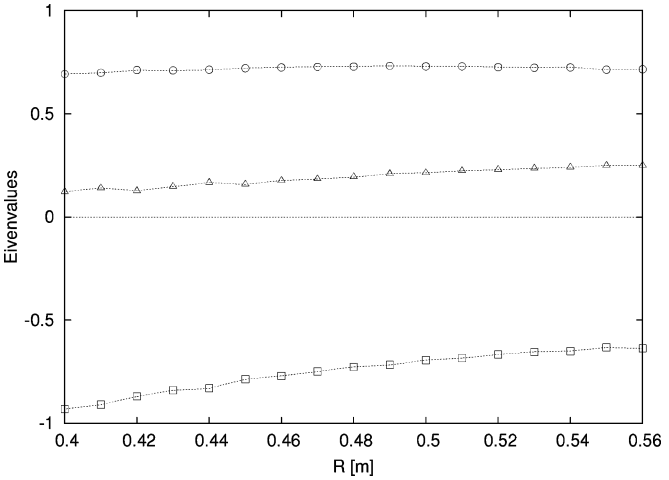


Fig. 14. Eigenvalues of $\nabla\boldsymbol{F}$ with respect to foot radius $R$.

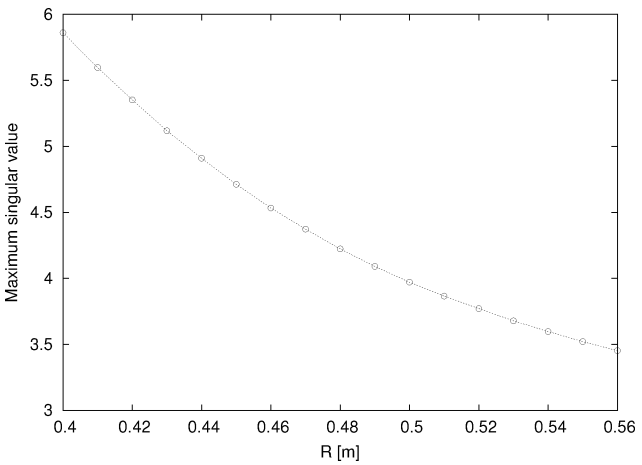


Fig. 15. Maximum singular value of $\nabla\boldsymbol{F}$ with respect to foot radius $R$.

Since $\nabla\boldsymbol{F} \in \mathbb{R}^{3\times3}$ has three eigenvalues and all of their magnitude should be less than one if the gait is stable.

Fig. 14 shows eigenvalues of $\nabla\boldsymbol{F}$ with respect to the foot radius $R$. All eigenvalues are real. One eigenvalue goes to $-1.0$ with the decrease in $R$, which implies that the gait stability grows worse; in other words, generating a one-periodic gait becomes difficult when $R$ is small. The limit cycle would exhibit period-doubling bifurcation.

Although eigenvalues of Poincaré return map is an indicator for limit cycle stability, we cannot evaluate its robustness. Robustness of gaits cannot be understood by only eigenvalues. Maximum singular value of $\nabla\boldsymbol{F}$ can be an indicator of robustness of the gait. The relation

$$\frac{\|\delta\boldsymbol{x}_{k+1}\|}{\|\delta\boldsymbol{x}_k\|} \leq \bar{\sigma}\left(\nabla\boldsymbol{F}\right) \tag{52}$$

holds in the error norm where $\bar{\sigma}$ means the maximum singular value. In $\bar{\sigma} < 1.0$, the error norm monotonically decreases and the gait stability or convergence speed is strong. Fig. 15 shows the maximum singular value of $\nabla\boldsymbol{F}$ with respect to $R$. We can see that it monotonically decreases with the increase in $R$, and it shows that robustness of a parametrically excited

gait is improved as the foot radius becomes larger. Theoretical investigation of the effect is left for future study.

## IX. Conclusion

This paper proposed a novel method of generating a biped gait based on the principle of parametric excitation. We also confirmed the validity of swing leg actuation through numerical simulations. A high-speed and energy-efficient gait was easily accomplished by pumping the swing leg. A parametric study was also undertaken to clarify the nature of the parametrically excited gait. Adjusting the foot radius had a strong effect on the walking speed because it dramatically decreased the energy dissipated by heel-strike collisions. Designing the optimal foot radius or shape that maximizes the effect of parametric excitation is one of the main subjects we intend to study in the future. We also found that energy efficiency can be improved by using elastic elements without changing the walking pattern. We also theoretically clarified the conditions necessary for maximum efficiency, and found that it is possible to achieve a minimum class of specific resistance by optimally adjusting mechanical impedances.

The greatest contribution of our study was achieving energy-efficient and high-speed dynamic biped locomotion without having to take ZMP conditions into account. We hope that our approach will provide new concepts for the introduction of *ZMP-free biped robots* as well as for the implementation of semicircular feet.

## Appendix

## Details of Equations

### A. Dynamic Equation

The details on the dynamic equation given by (7) are

$$\begin{bmatrix} M_{11} & M_{12} & M_{13} \\ & M_{22} & 0 \\ \text{Sym.} & & M_{33} \end{bmatrix} \ddot{\boldsymbol{q}} + \begin{bmatrix} h_1 \\ h_2 \\ h_3 \end{bmatrix} = \begin{bmatrix} 0 \\ 0 \\ 1 \end{bmatrix} u \tag{53}$$

where

$$\begin{aligned} M_{11} &= m(4R^2 - 2(a+l)R + a^2 + l^2 \\ &\quad + 2R(a+l-2R)\cos\theta_1) + I \\ M_{12} &= -mb_2((l-R)\cos(\theta_1-\theta_2) + R\cos\theta_2) \\ M_{13} &= m((l-R)\sin(\theta_1-\theta_2) - R\sin\theta_2) \\ M_{22} &= mb_2^2 + I \\ M_{33} &= m \\ h_1 &= -m(R(l-R)\dot\theta_1^2\sin\theta_1 \\ &\quad + 2\dot\theta_2\dot b_2((l-R)\cos(\theta_1-\theta_2) + R\cos\theta_2)) \\ &\quad - mb_2\dot\theta_2^2((l-R)\sin(\theta_1-\theta_2) - R\sin\theta_2) \\ &\quad - mg(a+l-2R)\sin\theta_1 \\ h_2 &= mb_2(2\dot b_2\dot\theta_2 + (l-R)\dot\theta_1^2\sin(\theta_1-\theta_2) + g\sin\theta_2) \\ h_3 &= m((l-R)\dot\theta_1^2\cos(\theta_1-\theta_2) - b_2\dot\theta_2^2 - g\cos\theta_2). \end{aligned}$$

### B. Transition Equation

Matrix $\bar{\boldsymbol{M}}(\bar{\boldsymbol{q}})$ in (9) is detailed as

$$\bar{\boldsymbol{M}}(\bar{\boldsymbol{q}}) = \begin{bmatrix} \boldsymbol{M}_1(\bar{\boldsymbol{q}}_1) & \boldsymbol{0}_{3\times3} \\ \boldsymbol{0}_{3\times3} & \boldsymbol{M}_2(\bar{\boldsymbol{q}}_2) \end{bmatrix} \tag{54}$$

$$\boldsymbol{M}_i(\bar{\boldsymbol{q}}_i) = \begin{bmatrix} m & 0 & m(a-R)\cos\theta_i \\ & m & -m(a-R)\sin\theta_i \\ \text{Sym.} & & I + m(a-R)^2 \end{bmatrix}. \tag{55}$$

The following describes the detailed derivation of $\boldsymbol{J}_I(\bar{\boldsymbol{q}})$ in (9) and (10). The velocity constraint conditions between the two legs to connect them are derived from geometric conditions such that, as shown in Fig. 3, the stance leg's hip is positioned the same as the swing leg's, and they can be expressed as

$$x_1 + (l-R)\sin\theta_1 = x_2 + (l-R)\sin\theta_2 \tag{56}$$

$$z_1 + (l-R)\cos\theta_1 = z_2 + (l-R)\cos\theta_2. \tag{57}$$

Their time derivatives yield following two conditions for velocity constraint:

$$\dot x_1^+ + (l-R)\dot\theta_1^+\cos\theta_1 = \dot x_2^+ + (l-R)\dot\theta_2^+\cos\theta_2 \tag{58}$$

$$\dot z_1^+ - (l-R)\dot\theta_1^+\sin\theta_1 = \dot z_2^+ - (l-R)\dot\theta_2^+\sin\theta_2. \tag{59}$$

The velocity constraint conditions, or the rolling contact conditions, on the other hand, between the stance leg and the ground are given by

$$\dot x_2^+ = R\dot\theta_2^+ \tag{60}$$

$$\dot z_2^+ = 0. \tag{61}$$

The Jacobian matrix, $\boldsymbol{J}_I(\bar{\boldsymbol{q}}) \in \mathbb{R}^{4\times6}$, which should satisfy $\boldsymbol{J}_I(\bar{\boldsymbol{q}})\dot{\bar{\boldsymbol{q}}}^+ = \boldsymbol{0}_{4\times1}$ is then formulated by summarizing the four conditions in (58)–(61) as

$$\boldsymbol{J}_I(\bar{\boldsymbol{q}}) = \begin{bmatrix} 1 & 0 & (l-R)\cos\theta_1 & -1 & 0 & -(l-R)\cos\theta_2 \\ 0 & 1 & -(l-R)\sin\theta_1 & 0 & -1 & (l-R)\sin\theta_2 \\ 0 & 0 & 0 & 0 & 1 & 0 \\ 0 & 0 & 0 & 1 & 0 & -R \end{bmatrix}. \tag{62}$$

## References


[1] H. Miura and I. Shimoyama, "Dynamic walk of a biped," *Int. J. Robot. Res.*, vol. 3, no. 2, pp. 60–74, Jun. 1984.

[2] A. Sano and J. Furusho, "Realization of natural dynamic walking using the angular momentum information," in *Proc. IEEE Int. Conf. Robot. Autom. (ICRA)*, Cincinnati, OH, May 13–18, 1990, vol. 3, pp. 1476–1481.

[3] S. Kajita, A. Kobayashi, and T. Yamaura, "Dynamic walking control of a biped robot along a potential energy conserving orbit," *IEEE Trans. Robot. Autom.*, vol. 8, no. 4, pp. 431–438, Aug. 1992.

[4] H. Hemami, F. C. Weimer, and S. H. Koozekanani, "Some aspects of the inverted pendulum problem for modeling of locomotion systems," *IEEE Trans. Autom. Control*, vol. AC-18, no. 6, pp. 658–661, Dec. 1973.

[5] M. Vukobratović and J. Stepanenko, "On the stability of anthropomorphic systems," *Math. Biosci.*, vol. 15, pp. 1–37, 1972.

[6] T. McGeer, "Passive dynamic walking," *Int. J. Robot. Res.*, vol. 9, no. 2, pp. 62–82, Apr. 1990.

[7] S. Collins, A. Ruina, R. Tedrake, and M. Wisse, "Efficient bipedal robots based on passive-dynamic walkers," *Sci.*, vol. 307, no. 5712, pp. 1082–1085, Feb. 2005.
[8] F. Asano, Z.-W. Luo, and M. Yamakita, "Biped gait generation and control based on a unified property of passive dynamic walking," *IEEE Trans. Robot.*, vol. 21, no. 4, pp. 754–762, Aug. 2005.
[9] F. Asano, Z.-W. Luo, and M. Yamakita, "Unification of dynamic gait generation methods via variable virtual gravity and its control performance analysis," in *Proc. IEEE/RSJ Int. Conf. Intell. Robots Syst. (IROS)*, Sep. 28–Oct. 2, 2004, vol. 4, pp. 3865–3870.
[10] T. Kinugasa, "Biped walking of EMU based on passive dynamic walking mechanism," in *Proc. ICASE/SICE Workshop Intell. Control Syst.*, Oct. 2002, pp. 304–309.
[11] H. Minakata and S. Tadakuma, "An experimental study of passive dynamic walking with non-rotate knee joint biped," in *Proc. ICASE/SICE Workshop Intell. Control Syst.*, Oct. 2002, pp. 298–303.
[12] E. K. Lavrovskii and A. M. Formalskii, "Optimal control of the pumping and damping of a swing," *J. Appl. Math. Mech.*, vol. 57, no. 2, pp. 311–320, 1993.
[13] R. Q. van der Linde, "Active leg compliance for passive walking," in *Proc. IEEE Int. Conf. Robot. Autom. (ICRA)*, Leuven, Belgium, May 16–20, 1998, vol. 3, pp. 2339–2345.
[14] K. Osuka and Y. Saruta, "Development and control of new legged robot quartet III—From active walking to passive walking," in *Proc. IEEE/RSJ Int. Conf. Intell. Robots Syst. (IROS)*, Takamatsu, Japan, Oct. 2000, vol. 2, pp. 991–995.
[15] R. Tedrake, T. W. Zhang, M. Fong, and H. S. Seung, "Actuating a simple 3D passive dynamic walker," in *Proc. IEEE Int. Conf. Robot. Autom. (ICRA)*, Apr. 26–May 1, 2004, vol. 5, pp. 4656–4661.
[16] M. Wisse, A. L. Schwab, R. Q. van der Linde, and F. C. T. van der Helm, "How to keep from falling forward: Elementary swing leg action for passive dynamic walkers," *IEEE Trans. Robot.*, vol. 21, no. 3, pp. 393–401, Jun. 2005.
[17] A. Goswami, B. Espiau, and A. Keramane, "Limit cycles in a passive compass gait biped and passivity-mimicking control laws," *J. Auton. Robots*, vol. 4, no. 3, pp. 273–286, Sep. 1997.
[18] M. Garcia, A. Chatterjee, and A. Ruina, "Efficiency, speed, and scaling of two-dimensional passive-dynamic walking," *Dyn. Stability Syst.*, vol. 15, no. 2, pp. 75–99, Jun. 2000.
[19] A. Goswami, B. Thuilot, and B. Espiau, "A study of the passive gait of a compass-like biped robot: Symmetry and chaos," *Int. J. Robot. Res.*, vol. 17, no. 12, pp. 1282–301, Dec. 1998.
[20] B. Thuilot, A. Goswami, and B. Espiau, "Bifurcation and chaos in a simple passive bipedal gait," in *Proc. IEEE Int. Conf. Robot. Autom. (ICRA)*, Albuquerque, NM, Apr. 20–25, 1997, vol. 1, pp. 792–798.

**Fumihiko Asano** (S'00–M'02) received the M.Eng. and Dr. Eng. degrees in control engineering from Tokyo Institute of Technology, Tokyo, Japan, in 1999 and 2002, respectively.

He is currently a Researcher with the Bio-Mimetic Control Research Center, Institute of Physical and Chemical Research (RIKEN), Nagoya, Japan. His current research interests include robotic legged locomotion, underactuated mechanical systems, and robotic dynamic manipulation.

Dr. Asano is a member of the Robotics Society of Japan (RSJ), the Society of Instrument and Control Engineers (SICE), and the Institute of Systems, Control, and Information Engineers (ISCIE).

**Zhi-Wei Luo** (M'94) received the B.E. degree in engineering from Huazhong University of Science and Technology, Wuhan, China, in 1984 and the M.Eng. and Dr. Eng. degrees in information engineering from Nagoya University, Nagoya, Japan, in 1991 and 1992, respectively.

From 1984 to 1986, he was a Teacher at Suzhou University, China. From 1986 to 1988, he was a Visiting Scholar with the Aichi Institute of Technology, Toyota, Japan. From 1992 to 1994, he was an Assistant Professor with Toyohashi University of Technology, Toyohashi, Japan. From 1994 to 1998, he was a Frontier Researcher with the Bio-Mimetic Control Research Center, Institute of Physical and Chemical Research (RIKEN), Nagoya, where since 2001, he has been the Laboratory Head of the Environment Adaptive Robotic Systems Laboratory, where he has led the development of a human interactive robot known as RI-MAN. From 1999 to 2001, he was an Associate Professor at Yamagata University, Yamagata. He is currently a Professor at Kobe University, Kobe, Japan. His current research interests include robotics, system control theory, and biomimetics.

Prof. Luo is a member of the Robotics Society of Japan (RSJ) and the Society of Instrument and Control Engineers (SICE). He is an Associate Editor of the IEEE TRANSACTIONS ON ROBOTICS.